Title

Traumatic brain injury metabolome and mitochondrial impact after early stage Ru360 treatment

Authors

Chitturi, Jyothsna
Santhakumar, Vijayalakshmi
Kannurpatti, Sridhar S

Publication Date

2021-03-01

DOI

10.1016/j.mito.2021.01.003

Peer reviewed

HHS Public Access

Author manuscript

Mitochondrion. Author manuscript; available in PMC 2022 March 01.

Published in final edited form as:

Mitochondrion. 2021 March ; 57: 192–204. doi:10.1016/j.mito.2021.01.003.

Traumatic brain injury metabolome and mitochondrial impact after early stage Ru360 treatment

Jyothsna Chitturi[1], **Vijayalakshmi Santhakumar**[2,3], **Sridhar S. Kannurpatti**[1,*]

[1]Department of Radiology, Rutgers New Jersey Medical School, Administrative Complex Building 5 (ADMC5), 30 Bergen Street Room 575, Newark, NJ 07101, USA.

[2]Department of Pharmacology, Physiology & Neuroscience, Rutgers New Jersey Medical School, MSB-H-512, 185 S. Orange Ave, Newark, NJ 07103, USA.

[3]Molecular, Cell and Systems Biology, University of California Riverside, Spieth 1308, 3401 Watkins Drive, Riverside, CA 92521, USA.

Abstract

Ru360, a mitochondrial Ca^{2+} uptake inhibitor, was tested in a unilateral fluid percussion TBI model in developing rats (P31). Vehicle and Ru360 treated TBI rats underwent sensorimotor behavioral monitoring between 24 to 72 hours, thereafter which 185 brain metabolites were analyzed postmortem using LC/MS. Ru360 treatment after TBI improved sensorimotor behavioral recovery, upregulated glycolytic and pentose phosphate pathways, mitigated oxidative stress and prevented NAD^+ depletion across both hemispheres. While neural viability improved ipsilaterally, it reduced contralaterally. Ru360 treatment, overall, had a global impact with most benefit near the strongest injury impact areas, while perturbing mitochondrial oxidative energetics in the milder TBI impact areas.

Keywords

traumatic brain injury; mitochondria; metabolomics; oxidative stress; Ru360; calcium uniporter

Introduction

Traumatic brain injury (TBI) is followed by excitotoxic secondary injury during the acute/subacute phase of a few hours to days due to diminished oxidative metabolism, oxidative stress, mitochondrial damage and neuronal death. Glutamatergic neurotransmission also gets

*Correspondence: Sridhar S. Kannurpatti, PhD, Department of Radiology, Rutgers Biomedical and Health Sciences, New Jersey Medical School, ADMC5, Room 575, 30 Bergen Street Newark, NJ07101, USA. kannursr@njms.rutgers.edu.

Author contributions: SK conceived and designed the study, JC and SK performed the experiments, JC analyzed data, VS contributed to significant laboratory resources and expertise for the rat model of Traumatic Brain Injury, JC and SK wrote the first draft of the manuscript and all authors edited and approved the submitted version of the manuscript.

Disclosure statement: All authors disclose that no competing financial interests exist

sensitized during this acute/subacute phase after a TBI, with molecular changes in the N-methyl-D-aspartate (NMDA) receptor subunits, leading to higher cytoplasmic and mitochondrial Ca^{2+} loads (Osteen, Giza et al. 2004). Higher cellular and mitochondrial Ca^{2+} loads after TBI (Yokobori, Mazzeo et al. 2014) is detrimental to mitochondrial survival and ascertains neuronal degeneration (Xiong, Gu et al. 1997, Verweij, Muizelaar et al. 2000, Fischer, Hylin et al. 2016). Hence, inhibiting mitochondrial Ca^{2+} uptake and cycling can prevent excitotoxic secondary neuronal injury (Giorgi, Agnoletto et al. 2012).

Mitochondrial membrane uncouplers, which depolarize the mitochondrial membrane potential to consequently inhibit mitochondrial Ca^{2+} uptake, have been tested earlier in preclinical TBI models (Pandya, Pauly et al. 2007, Pandya, Pauly et al. 2009). However, uncouplers have severe bioenergetic detriments which can exacerbate the preexisting TBI-induced brain energy metabolic crisis. Alternately, a direct inhibition of the mitochondrial Ca^{2+} uniporter channel complex (mCU) can diminish mitochondrial Ca^{2+} uptake without bioenergetic detriments and demonstrated using the compound Ru360, a specific inhibitor of the mCU (Kirichok, Krapivinsky et al. 2004), (Zhao, Li et al. 2015, Strokin and Reiser 2016). Mitochondrial Ca^{2+} uptake inhibition (if performed without any energetic stress or primary depolarization of the mitochondrial membrane potential), desensitizes plasma membrane ionotropic glutamate receptors (Budd and Nicholls 1996, Kannurpatti, Joshi et al. 2000, Strokin and Reiser 2016). One demonstrated mechanism is via a microdomain Ca^{2+} mediated negative feedback inhibition (Legendre, Rosenmund et al. 1993). Until such a re-evaluation of active mitochondrial control of cellular Ca^{2+} occurred, numerous earlier studies which blocked mitochondrial Ca^{2+} uptake (apparently using uncouplers) consistently observed increased cytoplasmic Ca^{2+} levels. This led to the notion of mitochondria as passive Ca^{2+} buffering organelles. With the re-evaluation of mitochondria as active regulators of cellular Ca^{2+} (Budd and Nicholls 1996, Kannurpatti, Joshi et al. 2000, Strokin and Reiser 2016), TBI treatments directly inhibiting mitochondrial Ca^{2+} uptake may provide dual benefits by not only preventing excessive mitochondrial Ca^{2+} overload, but also actively reducing glutamatergic neurotransmission.

Due to the vast mitochondrial functional diversity within the neural populations as the broad TBI pathophysiological process pans out (Lifshitz, Friberg et al. 2003, Park, Bell et al. 2008), oxidative stress from mitochondrial reactive oxygen species (ROS) will be relatively intense in regions close to the TBI epicenter. Hence, to mitigate oxidative stress and prevent detrimental downstream mitochondrial Ca^{2+} overload and secondary injury after TBI, mitochondrial Ca^{2+} uptake inhibition is a reasonable therapeutic strategy. However, mitochondrial Ca^{2+} uptake through the mCU is an essential process for normal ongoing oxidative energy metabolism (McCormack, Halestrap et al. 1990) and neural function (Kannurpatti and Biswal 2008, Fluegge, Moeller et al. 2012, Sanganahalli, Herman et al. 2013a, Kannurpatti, Sanganahalli et al. 2015, Kannurpatti 2017, Bas-Orth, Schneider et al. 2019). Therefore, mitochondrial Ca^{2+} uptake inhibition must be approached cautiously and beneficial only under conditions where the treatment does not perpetuate a universal brain-wide bioenergetic crisis, furthering mitochondrial damage (Pandya, Pauly et al. 2009). Hence, empirical dose range studies where mitochondrial Ca^{2+} uniporter inhibitors are protective *in vivo* and the thresholds beyond which inhibition of mitochondrial Ca^{2+} uptake

may become unfavorable or detrimental to global brain bioenergetics are critical to optimize TBI treatments.

Using Ru360, a highly specific mCU channel inhibitor (Matlib, Zhou et al. 1998), we have already established its dose dependent pharmacodynamic activity within the working brain *in vivo* (Sanganahalli, Herman et al. 2013a). Extracellular recordings from the somatosensory cortex failed to alter spontaneous and evoked neuronal electrical activities at doses of 120 μg/kg i.v. However, at higher doses of 240 μg/kg i.v, Ru360 significantly diminished stimulus-evoked neuronal electrical activity and the related blood oxygen level dependent (BOLD) responses and cerebral blood flow (CBF) responses measured by functional Magnetic Resonance Imaging (fMRI) (Sanganahalli, Herman et al. 2013a, Sanganahalli, Herman et al. 2013b). These findings led us to hypothesize that low dose Ru360 treatments (120 μg/kg), which mostly spares neuronal electrical activity while inhibiting neurovascular and neurometabolic activity (Sanganahalli, Herman et al. 2013a, Sanganahalli, Herman et al. 2013b), will improve TBI recovery. Using a rat model of fluid percussion TBI at the developmental age of P31, translating broadly to a 4–9 year range in humans (Clancy, Darlington et al. 2001), we tested the hypothesis by examining effects of Ru360 (120 μg/kg) or vehicle administered intraperitoneally at 30 min, 24 hours and 48 hours after TBI (ie., the acute/subacute window post injury. To capture the swathe of biochemical changes after TBI, which has a broad pathological consequence (Park, Bell et al. 2008), a metabolome wide investigation along with markers of neural viability and oxidative stress was performed and correlated with the neurological outcomes.

Methods and Materials

Animals

Male Sprague-Dawley rats (23–24 days old; weighing 60–80g) were procured from Charles River Laboratories, Wilmington, MA, USA and housed in pairs under controlled conditions. All procedures were approved by the Institutional Animal Care and Use Committee of Rutgers Biomedical and Health Sciences-Newark, New Jersey in accordance with the National Institute of Health policy on the use of research animals. Experimental procedures on animals were performed in accordance with the ARRIVE guidelines. Only male rats were used in the current study. This to avoid confounds of female hormonal and developmental differences between genders on the systemic level brain responses. Simple randomization was used to assign animal subjects to the different experimental groups. Blinding of behavioral measures was not performed as the same personnel performed the surgical and behavioral procedures on the animal groups. Animals were monitored within their cage environment daily throughout the duration of the experiments (Figure 1A).

Lateral fluid-percussion injury and pharmacological treatments

Rats at the age of 31 days (P31), underwent a lateral fluid percussion injury (FPI) as described previously (Chitturi, Li et al. 2018, Chitturi, Li et al. 2019, Chitturi, Santhakumar et al. 2019) and randomly assigned to the various treatments. Briefly, the FPI procedure was performed after a Luer-lock placement in rats anesthetized with Ketamine (80mg/kg i.p)-Xylazine (10mg/kg i.p). After a 3mm craniotomy on the left side of the skull −5 mm

posterior to the bregma and 3 mm lateral to the sagittal suture with intact dura, a luer-Lock syringe hub was glued using cyanoacrylate adhesive. TBI was performed 24 hours after luer-lock implantation using the FPI device (Virginia Commonwealth University, VA, USA) under 2% isoflurane anesthesia. A brief 20ms impact on the intact dura was made by a pendulum drop with an impact pressure of 1.8–2.0 atm measured by an extra-cranial transducer. Overall duration under isoflurane anesthesia for the FPI procedure was approximately 2–3 minutes. After injury, rats were monitored for the return of righting reflex and any signs of seizures for the next 30 minutes in a soft bedding cage. Typically, surgeries on animals were performed during the daytime between 9:00 am to 12:00 pm.

Ru360 or sterile saline-vehicle treatments were made through intraperitoneal injections of 120 μg/kg in three sessions starting from 30 mins, 24 hrs and 48 hrs after TBI. In both vehicle and Ru360 treated TBI groups, sensorimotor behavioral performance such as whisker stimulation induced motor response, forepaw stimulation induced motor response and forepaw utilization were determined during the acute/subacute window of 72-hours post-TBI. After completion of the behavioral measures at 72 hours, 183 metabolites were analyzed from the postmortem brain tissue using liquid chromatography/mass spectrometry (LC/MS). Both ipsilateral and contralateral hemisphere samples were metabolically analyzed due to the differential impact of the lateralized TBI on the brain as determined previously (Chitturi, Li et al. 2018).

Mortality rate of approximately 14% (2 out of 14 TBI animals) was observed throughout the current study. 2 TBI animals were lost, one at 24 hours after TBI without any treatment and another at 24 hours after first saline-vehicle dose. No mortality was observed in TBI animals treated with Ru360. 12 surviving animals were included in the study with 3 TBI animals without any treatment and 3 TBI animals with saline-vehicle treatments pooled together (n=6) forming the (no drug treated) TBI control group and TBI+Ru360 (n=6) forming the treatment group. No significant differences were observed in the metabolome between untreated and saline vehicle treated TBI animals as shown in the supplementary results (Figures S1 and S2), hence the two groups were pooled together forming the (no drug treated) TBI control group (n=6) for improved statistical power.

Liquid Chromatography/Mass Spectrometry (LC/MS)

72 hours after TBI, animals were euthanized by cervical dislocation and the brains rapidly removed (<60 seconds). Cerebellum and brain stem areas were removed, cerebral hemispheres separated across the midline, snap frozen in liquid nitrogen and stored at −80°C as described in our earlier study (Chitturi, Li et al. 2018). Brain tissue samples were weighed and disrupted in extraction buffer (80% methanol in water) using a micro-homogenizer. Each sample was transferred to a pre-cooled (dry ice) homogenization tube with 4 ml of pre-cooled 80% methanol and homogenized for 15 seconds using the standard micro homogenizer (Pro Scientific). 500μL of sample was taken out to a new Eppendorf tube centrifuged at 4°C for 15 minutes at 14,000 rpm. Supernatants were collected and normalized to tissue weight. LC/MS measurements were performed on the brain extract samples using a Q Exactive Orbitrap mass spectrometer (Thermo Scientific) coupled to a Vanquish UPLC system (Thermo Scientific) in a similar manner as our previous studies

(Chitturi, Li et al. 2018, Chitturi, Li et al. 2019, Chitturi, Santhakumar et al. 2019). The Q Exactive operated in a polarity-switching mode. A Sequant ZIC-HILIC column; 2.1/150mm i.d/length (Merck. Co, USA), was used for metabolite separation. Buffers consisted of high performance liquid chromatography (HPLC) buffer-A, which was 100% acetonitrile and HPLC buffer-B at pH=9.0 consisting of 95% (vol/vol) water, 5% (vol/vol) acetonitrile, 20mM ammonium hydroxide and 20 mM ammonium acetate. The flow rate was set at 150 μL/min with gradients from 85% to 30% for buffer A in 20 min followed by a 30% buffer A wash and re-equilibration with 85% buffer A. Metabolites were identified based on exact mass within 5 ppm and retention times (hence untargeted). A quality control (QC) sample was injected before each batch of biological samples to ensure the masses and retention times were accurate (Supplementary Figure S4). During data analysis, ion chromatograms from all LC-MS runs were aligned using a time dependent correction function to correct for minor retention time shifts across different samples. Relative metabolite quantification was performed based on peak area for each identified metabolite.

Metabolite Data analysis and statistics

Data analysis was performed using the software Metaboanalyst 3.0 (Xia, Psychogios et al. 2009, Xia, Sinelnikov et al. 2015). To minimize variations introduced during sample preparation effects of ion suppression, metabolite peak intensities were initially normalized to tissue wet weight. Due to deviations from normality as tested by Shapiro-Wilk's test, data were subsequently log transformed and auto-scaled (mean-centered and divided by the standard deviation of each variable) effectively converting them to Z-scores (Chitturi, Li et al. 2018, Chitturi, Santhakumar et al. 2019). Volcano plots of metabolites were determined and significantly changed metabolites were determined using a two-sample Student's t-test. A probability threshold of $P<0.05$ corrected for multiple comparisons using the false discovery rate (FDR) for type-1 error control was required for significance.

Partial least squares discriminant analysis (PLS-DA) was used to determine the separation between groups of the metabolite variables through rotation of the principal components obtained by PCA. This multivariate analysis was used due to the presence of more metabolite variables than observations in addition to correlation among the variables in the data (Tang, Peng et al. 2014). PLSDA 2D and 3D score plots were generated from the first two and first three principle components respectively for classification. The PLS-DA analysis was also used for feature selection and feature importance measures were generated (VIP: Variable Importance in Projection). R^2X and R^2Y, the fraction of variation that the model explains in the independent variables (X) and dependent variables (Y) and Q^2Y, the predictive accuracy of the model was estimated by the PLS-DA cross validation. These variables range between 0–1 with values >0.5 indicating good and >0.8 indicating outstanding predictive accuracy respectively. Loading plots (top 25 variables) were used to determine the clustering of variables and whether their relationship within (weightings) scores changed in response to Ru360 treatment.

Measuring the impact of individual metabolites on biochemical pathways, metabolic pathway analysis (MetPA) (Xia and Wishart 2010), and metabolite set enrichment analysis (MSEA) (Xia and Wishart 2010) were performed. MetPA combined the pathway enrichment

analysis and pathway topology analysis using a high-quality KEGG metabolic pathway database. For the MSEA, a preexisting rat reference library with global test algorithm along with the relative-between centrality algorithm for pathway topology analysis provided within the MetaboAnalyst software was used. Since many pathways were tested simultaneously, p-values were corrected for multiple comparisons using Holm-Bonferroni method (Holm P) and False Discovery Rate (FDR). In the pathway topology analysis degree centrality represents the number of links converging on a node and betweenness centrality represents the number of shortest paths passing through the node. MetPA analysis used betweenness centrality measure informing on the global network topology as implemented earlier (Chitturi, Li et al. 2018), distinct from the degree centrality measure which informed local connectivity.

MSEA characterizes functionally related metabolite sets without the need to preselect the metabolites based on some arbitrary cut-off threshold. Patterns of metabolites that are significantly enriched in biologically relevant pathways can be assessed (Xia and Wishart 2010). It has the potential to identify subtle but consistent changes among a group of related compounds in a certain biological pathway. A quantitative Enrichment Analysis (QEA) algorithm and a custom-made metabolite set library containing 36 metabolite sets based on metabolic pathways related to the detected brain metabolites, as implemented in our earlier studies (Chitturi, Li et al. 2018), was used as the reference library. The enrichment analyses considered reference metabolome built based on our analytical platform of the current targeted brain metabolites. A global test algorithm using a generalized linear model was used to estimate a Q-statistic for each metabolite set describing the correlation between metabolite concentration profiles (X) and physiological outcomes (Y). Q statistic for each metabolite was derived from the average of the Q statistics for each metabolite within the set. Statistical p-values after MSEA were corrected for multiple comparisons using the Holm-Bonferroni method (Holm P) and FDR.

NAA, GSH and GSSG were characterized within the large array of metabolites measured using LC/MS. After the first normalization using the wet weight of each sample a second normalization was performed to the respective peak height using the global mean of all metabolite peaks since the global mean did not show significant differences between untreated, vehicle treated or Ru360 treated conditions. Peak heights after the two-step normalization was used to estimate NAA, GSH and GSSG levels.

Whisker Stimulation-Induced Motor Response (WSIMR)

Extensive brain functional mapping in the whisker and forepaw representations, away from the injury epicenter has been characterized previously in the current TBI model along with sensorimotor behavioral outcomes to whisker stimuli or forepaw usage (Murugan, Santhakumar et al. 2016, Chitturi, Li et al. 2018). Hence for reproducibility and comparative analysis, WSIMR and Forelimb usage tests were adopted for the behavioral outcome measures. Furthermore, the first 72 hours of behavior was monitored to document the acute/subacute window of the fluid percussion TBI, during which secondary injury mechanisms manifest (Lifshitz, Friberg et al. 2003, Park, Bell et al. 2008, Lifshitz and Lisembee 2011) and most optimal for mitochondrially targeted treatments (Pandya, Pauly et al. 2009). Hence

behavioral tests were performed 24, 48, and 72hrs after injury, assessing sensorimotor deficits (Murugan, Santhakumar et al. 2016, Chitturi, Li et al. 2018).

During the WSIMR test, animals were placed in a test cage and left to habituate for 1min. Subsequently, whiskers on either side were stroked in a rostro-caudal direction using an applicator stick. Each trial consisted of multiple strokes at 3 Hz frequency and up to 10 trials on each side of the animal with an inter-trial gap of 1 min. Responses were scored on a scale of 0–5. Active avoidance by a quick backward head movement and away from the applicator stick followed by running away with 1–2 strokes = 5; quick backward head movement and away from the stroking stick with 1–2 strokes followed by a passive slow turn and walk away in a different direction = 4; slower head movement after 2–4 strokes away from the stick with a passive turn in a different direction =3; no backward head movement but only a slow head movement away from the stick after 4–8 strokes with no walk away = 2; no head movement, slow turn away or slow walk away reaction to stroking beyond 9 strokes = 0. All behaviors were scored live and the average score of 10 trials was considered.

For the forelimb usage test, each animal was observed for 5 minutes duration in a test cage 24, 48, and 72 hours after injury. Active exploration of vertical surfaces by rearing up on their hind limbs and wall surface exploration with their forelimbs were observed and scored. Number of independent wall placements observed for contralateral, ipsilateral, or both forelimbs were scored as a percentage of total forelimb wall placements. Percentage forelimb usage during an observation duration of 5 minutes was determined.

Results

The results summarize the behavioral and brain wide metabolome effects of Ru360 treatment made during the acute/subacute stage (0–72 hours) after a TBI.

Sensorimotor behaviors after Ru360 treatment

As previously established in the current model of TBI, no behavioral asymmetry or sensorimotor behavioral debilitation occurred in sham animals, whereas untreated TBI animals showed behavioral asymmetry with decreased ipsilateral-related WSIMR and spontaneous use of both forelimbs (Chitturi, Li et al. 2018). In the current study, untreated and vehicle treated TBI animals did not significantly differ in their WSIMR behaviors. Greater WSIMR deficit in response to tactile stimulation of the ipsilateral-related whiskers was observed when compared to contralateral-related whiskers. Ipsilateral-related whisker stimulation (right side of the animal; Figure 1B) activated the ipsilateral whisker representation based on the crossed pathway. Ipsilateral-related whisker stimulation led to significantly lower WSIMR compared to contralateral-related whisker stimulation (left side of the animal; Figure 1B) across untreated and vehicle treated TBI (Figure 2A, B). Ru360 treated TBI animals, however, showed significant improvement in both ipsilateral-related (Figure 2A) and contralateral-related whisker stimulation induced WSIMR at all time points compared to vehicle treated or untreated TBI (Figure 2B). Forelimb usage motor assessments across untreated TBI revealed a 46% spontaneous use of both forelimbs at all time points (Figure 2C), 34% use of only the contralateral-related forelimb, due to overuse of this forelimb after injury (Figure 2D) and less than 20% use of only the ipsilateral-related

forelimb (Figure 2E). Vehicle treated TBI also showed a similar trend of forelimb use as the untreated TBI (Figure 2C–E). Ru360 treated TBI, however, showed significant increase in the spontaneous use of both forelimbs (80%) (Figure 2C), normalized the overuse of the contralateral-related forelimb (Figure 2D) with no significant change in the ipsilateral-related forelimb use (Figure 2E). Overall, the improved WSIMR, spontaneous use of both forelimbs and normalization of contralateral-related forelimb use, combined with better behavioral symmetry across both sides after Ru360 treatment reached levels achieved by sham animals as observed previously (Chitturi, Li et al. 2018).

Effect of Ru360 treatment on the TBI metabolome

Metabolomic differences between the no drug treated TBI (untreated TBI and vehicle treated TBI groups combined) and Ru360 treated TBI animal group were determined by an untargeted multivariate analysis of 185 metabolites. Univariate analysis of the ipsilateral hemisphere (injury side; Figure 1B) in Ru360 treated TBI animals showed ≥ 2-fold change in 27 metabolites (~15% of the total identified metabolites) compared to no drug treated TBI. Among the 27 metabolites, 18 changed significantly (Figure 3A; $P<0.05$ corrected for multiple comparisons). Levels of N-acetylputrescine, $NADP^+$, AMP, betaine, phosphoenolpyruvic acid, NAD^+ and dimethylglycine increased with Ru360 treatment, whereas L-tryptophan, L-phenylalanine, oxidized glutathione (GSSG), pyro glutamic acid, s-adenosylhomocysteine, glycerol 3-phosphate, D-ribose 5-phosphate, dihydroxyacetone phosphate, glucose-1 phosphate, glucose-6 phosphate and glucosamine 6-phosphate levels decreased in Ru360 treated TBI (Figure 3A). Multivariate PLS-DA analysis showed distinct class separation with a highly accurate PLS-DA model (Accuracy=1.0, R^2 value=0.98, Q^2 value=0.83 (Figure 3B, C). MetPA indicated significant changes (Holm $P<0.05$) related to glycolysis, pentose phosphate pathway, nicotinate and nicotinamide metabolism, starch and sucrose metabolism, glutathione metabolism, glycine, serine and threonine metabolism, phenylalanine, tyrosine and tryptophan biosynthesis between the no drug TBI and Ru360 treated TBI (Figure 4A). MSEA analysis also showed significant (Holm $P<0.05$) enrichment in several critical metabolite clusters related to 27 metabolic pathways (Figure 4B). Prominent among these 27 metabolic pathways were cardiolipin biosynthesis, glycolysis, pentose phosphate pathway, gluconeogenesis, pyruvate metabolism, betaine, glutathione metabolism, phospholipid biosynthesis, TCA cycle and several amino acid (glutamate, phenylalanine, methionine, tryptophan, glycine, serine, tyrosine, arginine and proline) metabolism (Figure 4B). A separate comparison of the untreated TBI vs Ru360 treated TBI (Supplementary Figure S5) and vehicle treated TBI vs Ru360 treated TBI (Supplementary Figure S6) confirmed similar effects of Ru360 across the ipsilateral hemisphere.

On the contralateral hemisphere, Ru360 treated TBI showed ≥ 2-fold change in 32 metabolites (16.5% of the total targeted metabolites) compared to the no drug-treated TBI. Among the 32 metabolites with ≥ 2-fold change, 23 of them significantly changed (Figure 5A; $P<0.05$ corrected for multiple comparisons). N-acetylputrescine, NADP, AMP, citric acid, betaine, phosphoenolpyruvic acid, NAD, hexanoylcarnitine, propionylcarnitine, acetylcysteine and dimethylglycine increased with Ru360 treatment, whereas uric acid, phenylacetylglycine, caprylic acid, phenyllactic acid, oxaloacetic acid (OAA), quinolic acid, glucose-6 phosphate, nicotinic acid, methylacetoacetic acid, choline, L-histidinol and

pyruvic acid levels decreased with Ru360 treatment (Figure 5A). PLS-DA showed a distinct class separation with a highly accurate PLS-DA model (Accuracy=1.0, R^2 value=0.99, Q^2 value= 0.93 (Figure 5B, C). MetPA indicated significantly changed pathways (Holm $P<0.05$) related to nicotinate and nicotinamide metabolism, TCA cycle, glycine, serine, and threonine metabolism, glyoxylate and dicarboxylate metabolism, alanine, aspartate and glutamate metabolism and valine, leucine and isoleucine biosynthesis (Figure 6A). MSEA analysis also showed significant (Holm $P<0.05$) fold enrichment in several critical metabolite clusters related to 27 metabolic pathways with Ru360 treatment (Figure 6B). Prominent among these 27 metabolic pathways were betaine metabolism, lipid metabolism, pyruvate metabolism, TCA cycle, several amino acid metabolism (methionine, tryptophan, histidine, glycine, serine, phenylalanine, tyrosine, glutamate, arginine and proline), glycolysis, gluconeogenesis and pentose phosphate pathway (Figure 6B). A separate comparison of the untreated TBI vs Ru360 treated TBI (Supplementary Figure S7) and vehicle treated TBI vs Ru360 treated TBI (Supplementary Figure S8) confirmed similar effects of Ru360 across the contralateral hemisphere.

TBI induced changes in thiol redox state, NAA levels and the effect of Ru360

Ipsilateral fatty acid metabolism has been found to be severely perturbed leading to increased acyl carnitines, a hallmark of oxidative stress in the current TBI model (Chitturi, Li et al. 2018). Hence to test for antioxidative effects of Ru360, we measured the thiol redox state, ie., reduced to oxidized glutathione ratio (GSH/GSSG), a known biomarker of oxidative stress (Aoyama and Nakaki 2013). There was no difference in the thiol redox ratio between ipsilateral and contralateral hemispheres in the no drug treated TBI (Figure 7A). Ru360 treatment after TBI improved the thiol redox ratio (≈18 units) across both hemispheres (Figure 7A).

N-acetyl aspartate (NAA), a biomarker for neural (neural=neuronal+glial) viability (Marino, Zei et al. 2007, Moffett, Arun et al. 2013), (Demougeot, Garnier et al. 2001, Nordengen, Heuser et al. 2015) was measured. NAA levels in the present study was the highest in the contralateral TBI hemisphere (47±5; mean±SD) and reproducible from the contralateral NAA levels of 40±2 mean±SEM observed in our previous study in a different group of untreated TBI animals (Chitturi, Li et al. 2018). Ipsilateral NAA levels in the no drug treated TBI were 50% lower compared to the contralateral (Figure 7B), which reproduced the 50% ipsi-contra difference observed in untreated TBI animals observed previously (Chitturi, Li et al. 2018). While Ru360 treatment significantly diminished contralateral NAA to 34±3; mean ±SD from the no drug treated level of 47±5; mean±SD (Figure 7B), the ipsilateral impact was very different, where Ru360 significantly improved NAA to 35±4 when compared to 26±3 mean±SD in the no drug treated TBI animals (Figure 7B).

Discussion

A dose range of 40–320 μg/kg i.v Ru360 did not affect the vital physiological parameters or induce any change in the baseline cerebral blood flow as measured by functional laser Doppler Imaging (fLDI) in rats (Kanurpatti ad Biswal., 2008). In a subsequent study, we measured the pre-stimulus baseline cerebral blood flow after treatment with 120 or 240

μg/kg, i.v Ru360. In the fLDI measures, any cardiovascular effects can be sensitively captured via baseline cerebral blood flow changes. Again, no significant changes were observed with both doses of Ru360 treatments (Sanganahalli et al., 2013a). Hence, Ru360 at the dose of 120μg/kg i.p used in the current study was unlikely to produce significant perturbations in cardiac parameters and hence specific arrhythmic or bradycardia symptoms were not monitored in the Ru360 treated animals. Daily monitoring of animals also showed that they were overall healthy and active with no overt differences in grooming behavior or mobility between the Ru360 or vehicle treated TBI groups. Furthermore, no mortality was observed in TBI animals treated with Ru360.

No significant differences in the metabolome were observed in a larger sample of the same pediatric rat TBI model between untreated TBI and vehicle (saline+10% dimethyl sulphoxide) treated TBI (Chitturi, Santhakumar et al. 2019). As the current vehicle was only saline, we anticipated no significant differences between the vehicle treated and untreated TBI groups. Hence it was predetermined to use a minimum of n=3 animals in each group. As anticipated, we observed no significant brain metabolome differences between untreated and vehicle treated TBI animals (Supplementary data Figure S1 and S2). These two groups were subsequently pooled together to form the (no drug treated) TBI control group (n=6) for improved statistical power.

Significant sensorimotor behavioral debilitation across the side controlled by the ipsilateral brain representation correlated with both glycolytic and oxidative energy metabolic decline as previously established in this TBI model (Chitturi, Li et al. 2018). A similar lateralized sensorimotor behavioral debilitation and asymmetry was reproduced in the current study (Figure 2). Current results in P31 rats also concur with prior independent reports of acute/subacute stage lateral fluid percussion TBI in P27 rats, in which working memory debilitation correlated with diminished cerebral glucose metabolism (Prins and Hovda 2001). Hence, the energy metabolic decline may constitute one of the components affecting the acute/subacute stage sensorimotor behavior after TBI during development. Ru360 treatment rescued the acute/subacute stage sensorimotor behavioral deterioration after TBI when compared to the no drug treated TBI control groups (Figure 2).

The lateralized TBI maximally impacted the ipsilateral metabolome, neuronal survival, neural circuit function and sensorimotor behavior (Murugan, Santhakumar et al. 2016, Chitturi, Li et al. 2018, Parent, Li et al. 2019). Ipsilateral oxidative energy metabolism and glycolytic flux declined along with accumulation of many glycolytic intermediates and NAD^+ depletion (Chitturi, Li et al. 2018, Chitturi, Li et al. 2019). As observed in the current results, Ru360 treatment after TBI decreased ipsilateral glycolytic intermediates such as glucose-1-phosphate, glucose-6-phosphate and glucosamine-6-phosphate when compared to no drug treated TBI (Figure 8). These ipsilateral glycolytic intermediates typically increased after TBI when compared to sham (Chitturi, Li et al. 2018) and (Figure 8). Ru360 effect on ipsilateral glycolytic intermediates in the TBI brain maybe either due to improved utilization or decreased formation. However, given the pharmacological specificity of Ru360 to the mCU complex (Matlib, Zhou et al. 1998), and its ability to inhibit mitochondrial Ca^{2+} influx induced oxidative energy metabolism (McCormack, Halestrap et al. 1990), upregulation of brain glycolysis is likely during Ru360 treatment. Other ipsilateral glycolytic and pentose

phosphate pathway substrates such as glycerol-3-phosphate, dihydroxyacetone phosphate (DHAP) and D-ribose-5-phosphate were also lower (Figure 3A and Figure 8), indicating higher utilization after Ru360 treatment. Glycerol-3-phosphate converts to DHAP by dehydrogenation and subsequently DHAP enters the glycolytic pathway. As glycerol-3-phosphate and DHAP shuttle can rapidly (re)generate NAD^+ levels in the brain (Martano, Murru et al. 2016), their observed decrease along with NAD^+ increase with Ru360 treatment suggested a mitigation of the TBI induced ipsilateral energy metabolic decline by upregulation of glycolysis. Ru360's ability to decrease the overall neural, neurovascular and neurometabolic activity observed at the systems level within the normal adult brain (Kannurpatti and Biswal 2008, Sanganahalli, Herman et al. 2013a, Sanganahalli, Herman et al. 2013b), may also help reduce energy expenditure, thus mitigating the TBI-induced energy crisis ipsilaterally in the P31 rats. Although age is a caveat between adult and developing brain with respect to Ru360 effects, the directionality of Ru360's effects can be expected to remain the same.

An alternate source of NAD^+ biosynthesis is through the metabolism of the aromatic amino acid-tryptophan. As ipsilateral tryptophan levels were decreased after Ru360 treatment, its greater mobilization indicated an active alternate sustenance of NAD^+ production. Phenylalanine (with both glucogenic and ketogenic amino acid properties), whose catabolism provides energy supply during insufficiency, decreased ipsilaterally, indicating either its enhanced consumption or inhibited formation during mitochondrial inhibition with Ru360. Overall a lowered mitochondrial oxidative metabolic and higher glycolytic metabolic state with reduced glucogenic and ketogenic intermediates prevailed in the TBI brain ipsilaterally during Ru360 treatment when compared to no drug treatment.

TBI when left untreated or treated with vehicle led to severe perturbation of ipsilateral fatty acid metabolism with increased acyl carnitines, an indicator of increased oxidative stress (Chitturi, Li et al. 2018). Mitochondria are particularly vulnerable to high concentrations of acyl carnitines (Jones, McDonald et al. 2010) and restoration of the carnitine shuttle homeostasis through L-carnitine supplementation has been found to be neuroprotective (Ferreira and McKenna 2017). Ru360 did not significantly alter ipsilateral acyl carnitines, but strongly protected the thiol redox ratio (Figure 7A), indicating a significant ipsilateral antioxidative effect. Ru360 was also protective to ipsilateral neural populations (neural=neuronal+glial), preventing their further deterioration after TBI as observed by the significantly higher NAA levels between the (no drug treated) control TBI and Ru360 treated TBI groups (Figure 7B). As ipsilateral neural populations are relatively closer to the injury epicenter, they are more intensely affected by the bioenergetic crisis and dysfunctional mitochondria (Robertson, Saraswati et al. 2013, Prins and Matsumoto 2016, Prins 2017, Chitturi, Li et al. 2018). Amidst an already deteriorated ipsilateral oxidative metabolic level after TBI, further inhibitory effect of Ru360 on mitochondrial metabolism was not apparent. However, Ru360 treatment had the highest impact on ipsilateral one carbon metabolism, important for maintaining redox based defense mechanisms after injury. While ipsilateral betaine and dimethyl glycine increased, levels of S-adenosylhomocysteine decreased after Ru360 treatment (Figure 3A). Both betaine and dimethyl glycine are products of choline metabolism with antioxidative properties and cellular oxygenation enhancing ability (Bai, Xu et al. 2016, Zhang, Zhang et al. 2016). Based on these broad ipsilateral neurochemical

effects of Ru360, which prevented ipsilateral energetic decline and led to antioxidative and neuroprotective effects, very basic neural circuit activity would have been maintained to support essential sensorimotor behavior.

The lateralized TBI minimally impacted the contralateral brain metabolome with no significant changes in neural function or survival when compared to sham. Consequently, lower contralateral-related sensorimotor behavioral deficits were observed as established earlier (Murugan, Santhakumar et al. 2016, Chitturi, Li et al. 2018, Parent, Li et al. 2019). A similar pattern of milder contralateral-related sensorimotor behavioral deficit was reproduced in the current untreated and vehicle treated TBI rat groups (Figure 2B). Ru360 treatment after TBI significantly prevented the respective WSIMR declines on either side in addition to abolishing its inter-hemispheric asymmetry (Figure 2A,B). While the TBI-induced decline in the spontaneous use of both forelimbs (Figure 2C) and overuse of the contralateral-related forelimb (Figure 2D) was completely prevented with Ru360 treatment, the ipsilateral-related forelimb use was not significantly different between sham, TBI-untreated, TBI-vehicle treated or the TBI+Ru360 groups, probably owing to very small effect sizes (Figure 2E). Across the contralateral hemisphere, Ru360 treatment completely rescued the mild sensory (Figure 2B) and motor behavioral deficits (Figure 2D) despite an inhibition in the mostly normal contralateral mitochondrial oxidative metabolism after TBI (Figures 5 and 6). Although Ru360 decreased contralateral NAA levels (Figure 7B), indicating a diminished neural viability, it significantly improved the thiol redox state (Figure 7A). Hence, the contralateral neural populations (with relatively better functional mitochondria and functional neural circuits after TBI), although may receive antioxidative benefits, additionally encountered diminished oxidative metabolic capacity from Ru360-induced inhibition of mitochondrial Ca^{2+} influx (McCormack, Halestrap et al. 1990). Such a contralateral effect of Ru360 treatment *in vivo* suggests the delicate balance between optimal mitochondrial Ca^{2+} uptake and the maintenance of normal neural oxidative energy metabolism across the unaffected cellular populations after TBI, concurring with early mechanistic studies of this relationship *in vitro* (McCormack, Halestrap et al. 1990). Glutamate receptor signaling-dependent acceleration of energy metabolism being crucial for normal neurophysiological functions and maintenance of optimal neural bioenergetic capacity is well established (Kannurpatti, Joshi et al. 2000, Fluegge, Moeller et al. 2012, Strokin and Reiser 2016). Hence, the effect of mitochondrial Ca^{2+} uptake inhibition after Ru360 treatment may not significantly benefit energetically unaffected neural populations after TBI due to its net inhibitory effect on their normal mitochondrial oxidative metabolism. Probably, the mild contralateral oxidative metabolic decline in the Ru360 treated TBI brain prevented the contralateral-related forelimb overuse, which was similar to the sham level (Figure 2D). These differential effects of Ru360 across hemispheres suggest a TBI-induced mitochondrial functional diversity within the injured brain. Cellular populations relatively closer to the injury epicenter, affected by relatively greater injury-induced bioenergetic stress and contain more dysfunctional mitochondria, predominantly benefited from the Ru360 treatment. However, an improved thiol redox state across both hemispheres, suggested an overall antioxidative benefit accruing over the entire brain after Ru360 treatment.

Ru360 had a global effect commonly affecting many of the 27 pathways across hemispheres. However, there was a clear distinction on the intensity with which Ru360 impacted some of

the ipsilateral and contralateral biochemical pathways in the TBI brain. Ipsilaterally, Ru360 effects were more intense in upregulating cardiolipin biosynthesis, glycolysis, pentose phosphate pathway, gluconeogenesis, pyruvate metabolism, betaine metabolism and glutathione metabolism, but was less intense on glycolysis, pentose phosphate and gluconeogenesis contralaterally. A more intense effect on lipid metabolism, mitochondrial TCA cycle and transfer of acyl groups into mitochondria were observed contralaterally (not observed ipsilaterally), which strongly supports injury-induced mitochondrial functional diversity across the brain. The global effect of Ru360 on the brain was also evident from the relatively tight PLS-DA clustered Ru360 group when compared to controls (Figure 3B, C) and (Figure 5B, C). Although this seems like the control animals have a larger between subject variation, a closer comparison from our previous study on a different group of rats using the same TBI model indicated that the PLS-DA variability between sham animals or TBI animals were similar, with a wider cluster (Chitturi et al., 2018). Observing the PLS-DA results from Figure 3B, C and Figure 5B, C respectively, it is obvious that Ru360's inhibitory effect on brain mitochondria seems to cluster the metabolome between animals relatively tighter compared to the no-drug controls.

Differences in Ru360 efficacy in terms of pharmacokinetics (PK) and pharmacodynamics (PD) may arise due to the current intraperitoneal delivery as opposed to the intravenous delivery used earlier in normal rats (Kannurpatti and Biswal 2008, Sanganahalli, Herman et al. 2013a, Sanganahalli, Herman et al. 2013b). However, determining measurable neurochemical effects of Ru360 in a treatment regimen spread over 3 days, without overt inhibitory toxicity to the central nervous system was the original objective of this TBI study. Thus, based on our previous intravenous (i.v) dose studies of Ru360, we adopted the dose level 120 μg/kg using an intraperitoneal (i.p) delivery. While Ru360's PK/PD effects in the current i.p delivery will be potentially lesser than an i.v regimen, its metabolome-wide effect could be significantly discerned. The results provide valuable Ru360 dose threshold information of ≤ 120μg/kg i.p and suggests even lower doses for i.v delivery regimens to avoid mitochondrial damage.

Conclusions.

In summary, the mitochondrial Ca^{2+} uptake inhibitor, Ru360 at a dose of 120μg/kg i.p significantly improved neural viability and behavioral outcomes after TBI in developing rats. Ru360's ability to upregulate glycolytic energy metabolism and preserve thiol redox state improved the acute/subacute stage neural viability and sensorimotor behavior after TBI. Ru360's systemic response highlighted a functionally diverse mitochondrial population in the acute/subacute stage TBI brain. Ru360 treatment metabolically perturbing unaffected neural populations far away from the injury epicenter, indicated that lower doses need to be considered for optimal therapeutic effect while avoiding excess mitochondrial inhibition and neural damage.

Supplementary Material

Refer to Web version on PubMed Central for supplementary material.

Acknowledgements:

This study was supported by funding from the New Jersey Commission for Brain injury research (CBIR15IRG010; SK) and National Institutes of Health (R01NS097750; VS). Sample preparation and the LC/MS measurements were performed at the Proteomics and Metabolomics Core Facility at Weill Cornell Medicine, NY.

Abbreviations:

TBI	Traumatic brain injury
LC/MS	Liquid Chromatography/Mass Spectrometry
NAD^+	Nicotinamide adenine dinucleotide oxidized form
Ca^{2+}	calcium ion
FPI	Fluid percussion injury
PL-SDA	Partial least squares discriminant analysis
MSEA	Metabolite set enrichment analysis
NAA	N-acetyl-aspartate
GSH	Glutathione reduced form
GSSG	Glutathione oxidized form
NMDA	N-methyl-D-aspartate
mCU	mitochondrial Ca^{2+} uniporter
ROS	Reactive oxygen species
CBF	Cerebral blood flow
BOLD	Blood oxygen level dependent
fMRI	Functional magnetic resonance imaging
WSIMR	Whisker stimulation induced motor response

References

Aoyama K and Nakaki T (2013). “Impaired Glutathione Synthesis in Neurodegeneration.” International Journal of Molecular Sciences 14(10): 21021–21044. [PubMed: 24145751]

Bai K, Xu W, Zhang J, Kou T, Niu Y, Wan X, Zhang L, Wang C and Wang T (2016). “Assessment of Free Radical Scavenging Activity of Dimethylglycine Sodium Salt and Its Role in Providing Protection against Lipopolysaccharide-Induced Oxidative Stress in Mice.” PLoS One 11(5): e0155393. [PubMed: 27171376]

Bas-Orth C, Schneider J, Lewen A, McQueen J, Hasenpusch-Theil K, Theil T, Hardingham GE, Bading H and Kann O (2019). “The mitochondrial calcium uniporter is crucial for the generation of fast cortical network rhythms.” J Cereb Blood Flow Metab: 271678X19887777.

Budd SL and Nicholls DG (1996). “Mitochondria, calcium regulation, and acute glutamate excitotoxicity in cultured cerebellar granule cells.” J Neurochem 67(6): 2282–2291. [PubMed: 8931459]

Chitturi J, Li Y, Santhakumar V and Kannurpatti SS (2018). “Early behavioral and metabolomic change after mild to moderate traumatic brain injury in the developing brain.” Neurochem Int 120: 75–86. [PubMed: 30098378]

Chitturi J, Li Y, Santhakumar V and Kannurpatti SS (2019). “Consolidated Biochemical Profile of Subacute Stage Traumatic Brain Injury in Early Development.” Frontiers in Neuroscience 13.

Chitturi J, Santhakumar V and Kannurpatti SS (2019). “Beneficial Effects of Kaempferol after Developmental Traumatic Brain Injury Is through Protection of Mitochondrial Function, Oxidative Metabolism, and Neural Viability.” J Neurotrauma 36(8): 1264–1278. [PubMed: 30430900]

Clancy B, Darlington RB and Finlay BL (2001). “Translating developmental time across mammalian species.” Neuroscience 105(1): 7–17. [PubMed: 11483296]

Demougeot C, Garnier P, Mossiat C, Bertrand N, Giroud M, Beley A and Marie C (2001). “N-Acetylaspartate, a marker of both cellular dysfunction and neuronal loss: its relevance to studies of acute brain injury.” J Neurochem 77(2): 408–415. [PubMed: 11299303]

Ferreira GC and McKenna MC (2017). “L-Carnitine and Acetyl-L-carnitine Roles and Neuroprotection in Developing Brain.” Neurochemical research 42(6): 1661–1675. [PubMed: 28508995]

Fischer TD, Hylin MJ, Zhao J, Moore AN, Waxham MN and Dash PK (2016). “Altered Mitochondrial Dynamics and TBI Pathophysiology.” Front Syst Neurosci 10: 29. [PubMed: 27065821]

Fluegge D, Moeller LM, Cichy A, Gorin M, Weth A, Veitinger S, Cainarca S, Lohmer S, Corazza S, Neuhaus EM, Baumgartner W, Spehr J and Spehr M (2012). “Mitochondrial Ca(2+) mobilization is a key element in olfactory signaling.” Nat Neurosci 15(5): 754–762. [PubMed: 22446879]

Giorgi C, Agnoletto C, Bononi A, Bonora M, De Marchi E, Marchi S, Missiroli S, Patergnani S, Poletti F, Rimessi A, Suski JM, Wieckowski MR and Pinton P (2012). “Mitochondrial calcium homeostasis as potential target for mitochondrial medicine.” Mitochondrion 12(1): 77–85. [PubMed: 21798374]

Jones LL, McDonald DA and Borum PR (2010). “Acylcarnitines: role in brain.” Prog Lipid Res 49(1): 61–75. [PubMed: 19720082]

Kannurpatti SS (2017). “Mitochondrial calcium homeostasis: Implications for neurovascular and neurometabolic coupling.” Journal of Cerebral Blood Flow and Metabolism 37(2): 381–395. [PubMed: 27879386]

Kannurpatti SS and Biswal BB (2008). “Mitochondrial Ca2+ uniporter blockers influence activation-induced CBF response in the rat somatosensory cortex.” J Cereb Blood Flow Metab 28(4): 772–785. [PubMed: 17971788]

Kannurpatti SS, Joshi PG and Joshi NB (2000). “Calcium sequestering ability of mitochondria modulates influx of calcium through glutamate receptor channel.” Neurochem Res 25(12): 1527–1536. [PubMed: 11152381]

Kannurpatti SS, Sanganahalli BG, Herman P and Hyder F (2015). “Role of mitochondrial calcium uptake homeostasis in resting state fMRI brain networks.” NMR Biomed.

Kirichok Y, Krapivinsky G and Clapham DE (2004). “The mitochondrial calcium uniporter is a highly selective ion channel.” Nature 427(6972): 360–364. [PubMed: 14737170]

Legendre P, Rosenmund C and Westbrook GL (1993). “Inactivation of NMDA channels in cultured hippocampal neurons by intracellular calcium.” J Neurosci 13(2): 674–684. [PubMed: 7678859]

Lifshitz J, Friberg H, Neumar RW, Raghupathi R, Welsh FA, Janmey P, Saatman KE, Wieloch T, Grady MS and McIntosh TK (2003). “Structural and functional damage sustained by mitochondria after traumatic brain injury in the rat: evidence for differentially sensitive populations in the cortex and hippocampus.” J Cereb Blood Flow Metab 23(2): 219–231. [PubMed: 12571453]

Lifshitz J and Lisembee AM (2011). “Neurodegeneration in the somatosensory cortex after experimental diffuse brain injury.” Brain Struct Funct 217(1): 49–61. [PubMed: 21597967]

Marino S, Zei E, Battaglini M, Vittori C, Buscalferri A, Bramanti P, Federico A and De Stefano N (2007). “Acute metabolic brain changes following traumatic brain injury and their relevance to clinical severity and outcome.” J Neurol Neurosurg Psychiatry 78(5): 501–507. [PubMed: 17088335]

Martano G, Murru L, Moretto E, Gerosa L, Garrone G, Krogh V and Passafaro M (2016). "Biosynthesis of glycerol phosphate is associated with long-term potentiation in hippocampal neurons." Metabolomics 12: 133. [PubMed: 27499721]

Matlib MA, Zhou Z, Knight S, Ahmed S, Choi KM, Krause-Bauer J, Phillips R, Altschuld R, Katsube Y, Sperelakis N and Bers DM (1998). "Oxygen-bridged dinuclear ruthenium amine complex specifically inhibits Ca2+ uptake into mitochondria in vitro and in situ in single cardiac myocytes." J Biol Chem 273(17): 10223–10231. [PubMed: 9553073]

McCormack JG, Halestrap AP and Denton RM (1990). "Role of calcium ions in regulation of mammalian intramitochondrial metabolism." Physiol Rev 70(2): 391–425. [PubMed: 2157230]

Moffett JR, Arun P, Ariyannur PS and Namboodiri AM (2013). "N-Acetylaspartate reductions in brain injury: impact on post-injury neuroenergetics, lipid synthesis, and protein acetylation." Front Neuroenergetics 5: 11. [PubMed: 24421768]

Murugan M, Santhakumar V and Kannurpatti S (2016). "Facilitating mitochondrial calcium uptake improves activation-induced cerebral blood flow and behaviour after mTBI." Frontiers in Neuroscience.

Nordengen K, Heuser C, Rinholm JE, Matalon R and Gundersen V (2015). "Localisation of N-acetylaspartate in oligodendrocytes/myelin." Brain Struct Funct 220(2): 899–917. [PubMed: 24379086]

Osteen CL, Giza CC and Hovda DA (2004). "Injury-induced alterations in N-methyl-D-aspartate receptor subunit composition contribute to prolonged 45calcium accumulation following lateral fluid percussion." Neuroscience 128(2): 305–322. [PubMed: 15350643]

Pandya JD, Pauly JR, Nukala VN, Sebastian AH, Day KM, Korde AS, Maragos WF, Hall ED and Sullivan PG (2007). "Post-Injury Administration of Mitochondrial Uncouplers Increases Tissue Sparing and Improves Behavioral Outcome following Traumatic Brain Injury in Rodents." J Neurotrauma 24(5): 798–811. [PubMed: 17518535]

Pandya JD, Pauly JR and Sullivan PG (2009). "The optimal dosage and window of opportunity to maintain mitochondrial homeostasis following traumatic brain injury using the uncoupler FCCP." Exp Neurol 218(2): 381–389. [PubMed: 19477175]

Parent M, Li Y, Santhakumar V, Hyder F, Sanganahalli BG and Kannurpatti SS (2019). "Alterations of Parenchymal Microstructure, Neuronal Connectivity, and Cerebrovascular Resistance at Adolescence after Mild-to-Moderate Traumatic Brain Injury in Early Development." J Neurotrauma 36(4): 601–608. [PubMed: 29855211]

Park E, Bell JD and Baker AJ (2008). "Traumatic brain injury: Can the consequences be stopped?" Canadian Medical Association Journal 178(9): 1163–1170. [PubMed: 18427091]

Prins ML (2017). "Glucose metabolism in pediatric traumatic brain injury." Childs Nerv Syst 33(10): 1711–1718. [PubMed: 29149386]

Prins ML and Hovda DA (2001). "Mapping cerebral glucose metabolism during spatial learning: interactions of development and traumatic brain injury." J Neurotrauma 18(1): 31–46. [PubMed: 11200248]

Prins ML and Matsumoto J (2016). "Metabolic Response of Pediatric Traumatic Brain Injury." J Child Neurol 31(1): 28–34. [PubMed: 25336427]

Robertson CL, Saraswati M, Scafidi S, Fiskum G, Casey P and McKenna M (2013). "Cerebral Glucose Metabolism in an Immature Rat Model of Pediatric Traumatic Brain Injury." JOURNAL OF NEUROTRAUMA 30: 6.

Sanganahalli BG, Herman P, Hyder F and Kannurpatti SS (2013a). "Mitochondrial calcium uptake capacity modulates neocortical excitability." J Cereb Blood Flow Metab 33(7): 1115–1126. [PubMed: 23591650]

Sanganahalli BG, Herman P, Hyder F and Kannurpatti SS (2013b). "Mitochondrial functional state impacts spontaneous neocortical activity and resting state FMRI." PLoS One 8(5): e63317. [PubMed: 23650561]

Strokin M and Reiser G (2016). "Mitochondrial Ca2+ Processing by a Unit of Mitochondrial Ca2+ Uniporter and Na+/Ca2+ Exchanger Supports the Neuronal Ca2+ Influx via Activated Glutamate Receptors." Neurochemical Research 41(6): 1250–1262. [PubMed: 26842930]

Tang L, Peng S, Bi Y, Shan P and Hu X (2014). “A new method combining LDA and PLS for dimension reduction.” PLoS One 9(5): e96944. [PubMed: 24820185]

Verweij BH, Muizelaar JP, Vinas FC, Peterson PL, Xiong Y and Lee CP (2000). “Impaired cerebral mitochondrial function after traumatic brain injury in humans.” J Neurosurg 93(5): 815–820. [PubMed: 11059663]

Xia J, Psychogios N, Young N and Wishart DS (2009). “MetaboAnalyst: a web server for metabolomic data analysis and interpretation.” Nucleic Acids Res 37(Web Server issue): W652–660. [PubMed: 19429898]

Xia J, Sinelnikov IV, Han B and Wishart DS (2015). “MetaboAnalyst 3.0--making metabolomics more meaningful.” Nucleic Acids Res 43(W1): W251–257. [PubMed: 25897128]

Xia J and Wishart DS (2010). “MetPA: a web-based metabolomics tool for pathway analysis and visualization.” Bioinformatics 26(18): 2342–2344. [PubMed: 20628077]

Xia J and Wishart DS (2010). “MSEA: a web-based tool to identify biologically meaningful patterns in quantitative metabolomic data.” Nucleic Acids Res 38(Web Server issue): W71–77. [PubMed: 20457745]

Xiong Y, Gu Q, Peterson PL, Muizelaar JP and Lee CP (1997). “Mitochondrial dysfunction and calcium perturbation induced by traumatic brain injury.” J Neurotrauma 14(1): 23–34. [PubMed: 9048308]

Yokobori S, Mazzeo AT, Gajavelli S and Bullock MR (2014). “Mitochondrial neuroprotection in traumatic brain injury: rationale and therapeutic strategies.” CNS Neurol Disord Drug Targets 13(4): 606–619. [PubMed: 24168363]

Zhang M, Zhang H, Li H, Lai F, Li X, Tang Y, Min T and Wu H (2016). “Antioxidant Mechanism of Betaine without Free Radical Scavenging Ability.” J Agric Food Chem 64(42): 7921–7930. [PubMed: 27677203]

Zhao LT, Li SH, Wang SL, Yu N and Liu J (2015). “The effect of mitochondrial calcium uniporter on mitochondrial fission in hippocampus cells ischemia/reperfusion injury.” Biochemical and Biophysical Research Communications 461(3): 537–542. [PubMed: 25911325]

- Ru360 improved sensorimotor behavioral recovery in developing age Traumatic Brain Injured rats
- Ru360 treatment of Traumatic Brain Injured rats upregulated non-oxidative metabolism along with antioxidative effects
- While Ru360 was beneficial to ipsilateral neural viability in the injured brain, it was not beneficial contralaterally.
- Brain mitochondrial functional diversity after unilateral Traumatic Brain Injury demonstrated

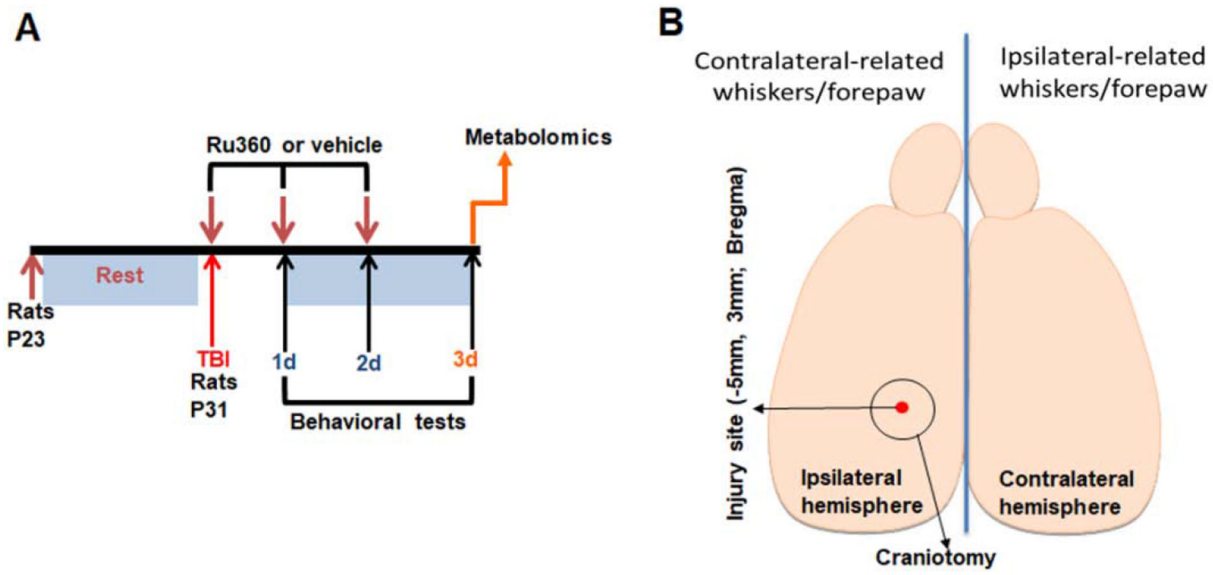

Figure 1.

A) Schematic of the experimental design depicting the Ru360 or vehicle treatment regimen after TBI and the behavioral and metabolomic assessment time points. **B**) Schematic of the rat brain indicating the stereotaxic location of the lateralized fluid percussion induced TBI and craniotomy.

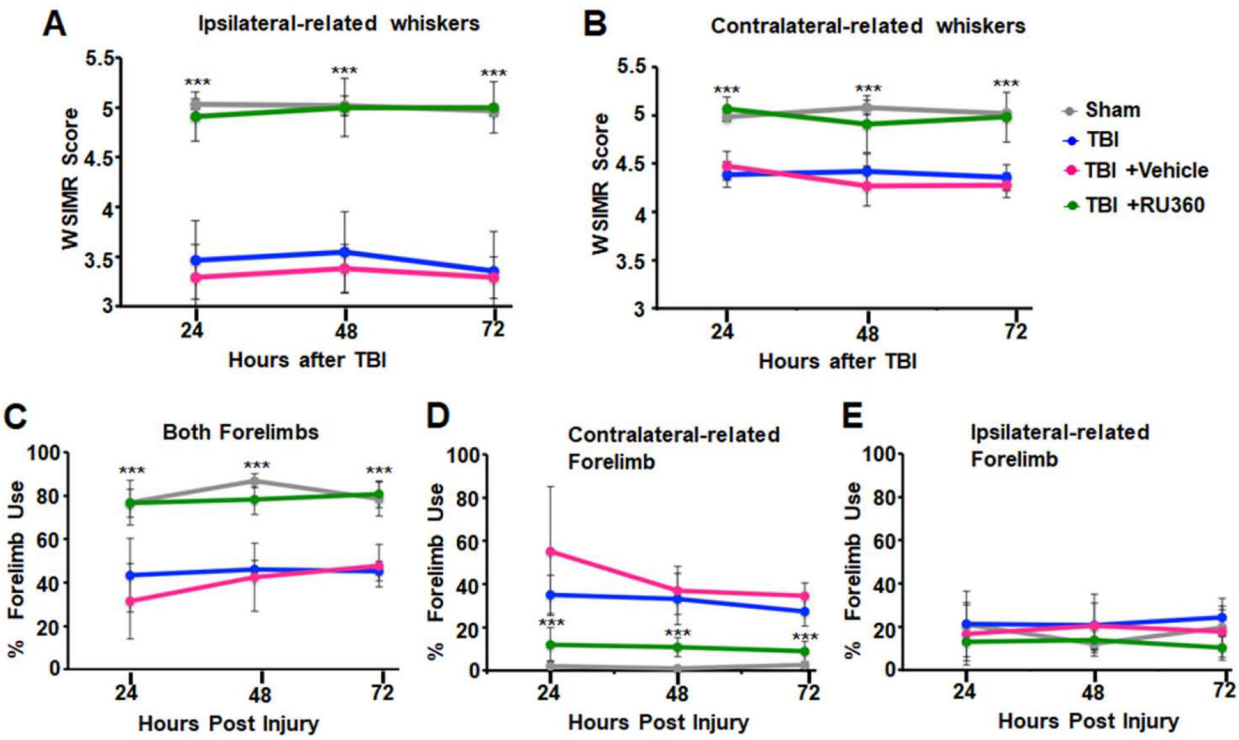

Figure 2. Improved sensorimotor behaviors after Ru360 treatment

A) During ipsilateral-related whisker stimulation, untreated TBI (blue; n=3) and vehicle-treated TBI animals (pink; n=3) had highest WSIMR reductions with no significant difference between them. Ru360 treatment significantly improved WSIMR (green; n=6), which was comparable to the sham levels (dashed line); data from our previous study under similar conditions (Chitturi, Li et al. 2018). Significantly different ***p<0.0001; df=1; F=511.53 two-way ANOVA with repeated measures. **B**) During contralateral-related whisker stimulation, lesser WSIMR decrease was observed in the untreated TBI and vehicle treated TBI. A significant WSIMR improvement occurred in the TBI+Ru360 group, which was comparable to sham levels (dashed line). Significantly different ***p<0.0001; df=1; F=18.94 two-way ANOVA with repeated measures. **C)** Similar to shams (grey line), Ru360 treated TBI animals (green; n=6) spontaneously used both forelimbs more frequently (80%). This was significantly higher compared to untreated TBI (46%) (blue; n=3) or vehicle treated TBI (34%) (pink; n=3). Significantly different ***p<0.0001; df=1; F=83.09 two-way ANOVA with repeated measures. **D)** Untreated and vehicle treated TBI animals used only the contralateral-related forelimb 40% of the time with no significant difference between them. However, Ru360 treatment, reduced its usage to 10%, which was comparable to the sham level (grey line) and consistent with its effect of improving simultaneous usage of both forelimbs. Significantly different ***p<0.0001; df=1; F=44.17 two-way ANOVA with repeated measures. **E)** Compared to sham levels of 5% usage of the ipsilateral-related forelimbs (grey line), a 20% usage was observed in the untreated and vehicle treated TBI groups with no significant difference between them. TBI+Ru360 treatment showed no significant difference compared to the untreated or vehicle-treated TBI in the ipsilateral-related forelimb use, but was significantly higher than the sham level (grey line). Data

represent mean±SD. A subject-wise representation of this data across animals is provided in the supplementary Figure S3.

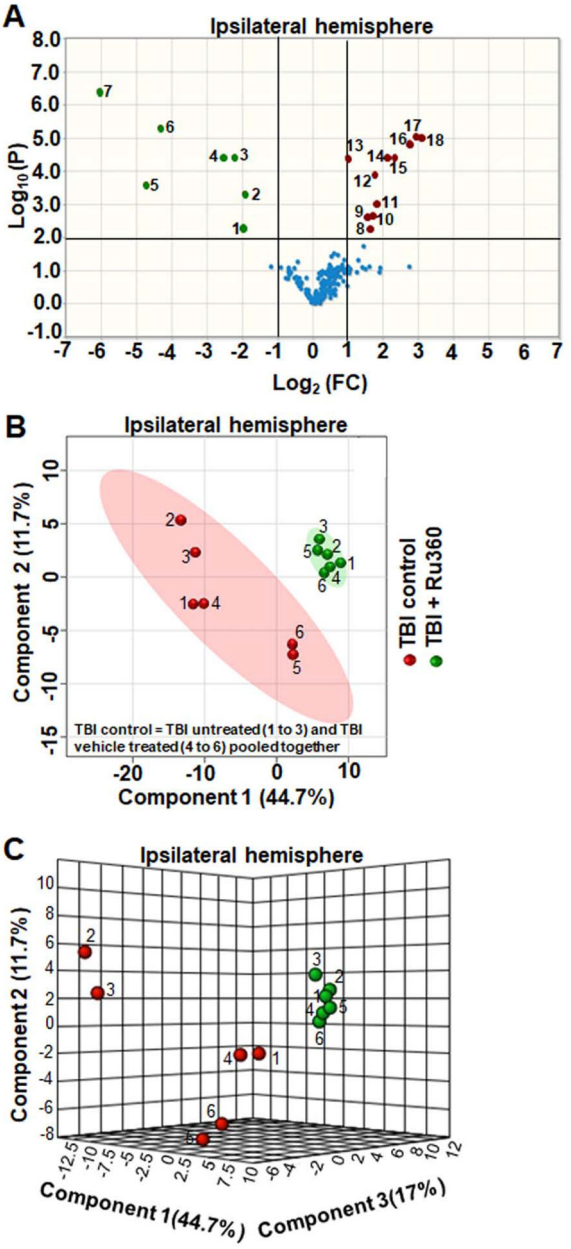

No	Metabolite
1	N-acetylputrescine
2	NADP
3	AMP
4	Betaine
5	Phosphoenolpyruvic acid
6	NAD
7	Dimethylglycine
8	Glycerol-3-phosphate
9	L-tryptophan
10	Oxidized glutathione (GSSG)
11	Pyroglutamic acid
12	S-adenosylhomocysteine
13	Dihydroxyacetone phosphate
14	L-phenylalanine
15	D-ribose 5-phosphate
16	Glucose-1-phosphate
17	Glucosamine-6-phosphate
18	Glucose-6-phosphate

Figure 3. Ru360 treatment on the ipsilateral hemisphere TBI metabolome

A) Volcano plot showing fold changes (FC) on the x-axis and FDR adjusted p-values on the y-axis. Black vertical and horizontal lines reflect the threshold criteria (FC=1.0 and $p<0.05$). Green and red dots represent metabolites which significantly increased or decreased after Ru360 treatment respectively. 8% of the metabolites significantly changed between TBI +Ru360 treated (n=6) and control TBI animals (n=6). Table on the right indicates significantly changed metabolites as numbered in the volcano plot on the left panel. **B**) PLS-DA 2D scores plot and **C**) PLS-DA 3D scores plot respectively, indicating a complete class separation between Ru360 treated TBI (green dots) versus control TBI animals (red dots) with a tight clustering of the TBI metabolome across the Ru360 treated animals.

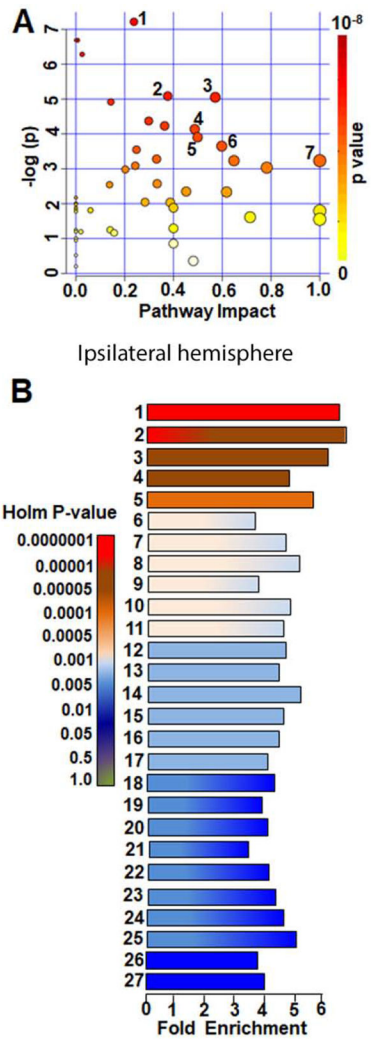

No	Metabolic pathway/Metabolism	P value	Holm P	FDR	Impact
1	Glycolysis or Gluconeogenesis	0.0000005	0.00002	0.00002	0.23
2	Pentose phosphate pathway	0.00003	0.001	0.0003	0.37
3	Nicotinate and nicotinamide	0.00004	0.001	0.0003	0.57
4	Starch and sucrose metabolism	0.0002	0.009	0.001	0.48
5	Glutathione metabolism	0.0004	0.01	0.001	0.49
6	Glycine, serine and threonine	0.0006	0.02	0.002	0.59
7	Phenylalanine, tyrosine and tryptophan biosynthesis	0.001	0.05	0.004	1.0

No	Metabolite set	P value	Holm P	FDR
1	Cardiolipin biosynthesis	0.000000003	0.0000001	0.0000001
2	Glycolysis	0.0000007	0.00003	0.00001
3	Pentose phosphate pathway	0.000001	0.00004	0.00001
4	Gluconeogenesis	0.000002	0.00007	0.00002
5	Pyruvate metabolism	0.000004	0.0001	0.00003
6	Betaine metabolism	0.00003	0.001	0.0002
7	Glutathione metabolism	0.00004	0.001	0.0002
8	Glutamate metabolism	0.00004	0.001	0.0002
9	Methionine metabolism	0.00005	0.001	0.0002
10	Tryptophan metabolism	0.00007	0.001	0.0002
11	Phospholipid biosynthesis	0.00007	0.001	0.0002
12	Histidine metabolism	0.00009	0.002	0.0002
13	Citric acid cycle	0.0001	0.002	0.0002
14	Phenylalanine and tyrosine metabolism	0.0001	0.003	0.0003
15	Tyrosine metabolism	0.0002	0.004	0.0005
16	Nicotinate and nicotinamide metabolism	0.0002	0.004	0.0005
17	Glycine and serine metabolism	0.0002	0.004	0.0005
18	Purine metabolism	0.0005	0.01	0.001
19	Ammonia recycling	0.0006	0.01	0.001
20	Glucose alanine cycle	0.0008	0.01	0.001
21	Urea cycle	0.0008	0.01	0.001
22	Aminosugar metabolism	0.0009	0.01	0.001
23	Transfer of acetyl groups into mitochondria	0.001	0.01	0.001
24	Oxidative and mitochondrial metabolism	0.001	0.01	0.001
25	Lipid metabolism	0.001	0.01	0.002
26	Malate-aspartate shuttle	0.003	0.03	0.004
27	Spermidine and spermine biosynthesis	0.004	0.03	0.004

Figure 4. Pathway analysis of control versus Ru360 treatment on the ipsilateral hemisphere

A) Left-panel: Pathway analysis using MetPA with node colors indicating uncorrected p-values and node size the pathway impact values. Right-panel: Table showing significantly changed metabolic pathways with a threshold of $p<0.05$ for the corrected Holm p-value. **B**) Left-panel: MSEA results with y-axis indicating the significantly different metabolite sets based on a threshold of $p<0.05$ for the Holm p-value and color scaled to the corrected Holm p-value and x-axis indicating the respective fold enrichment. Right-panel: Table showing affected pathways relevant to the significantly enriched metabolite sets determined by MSEA.

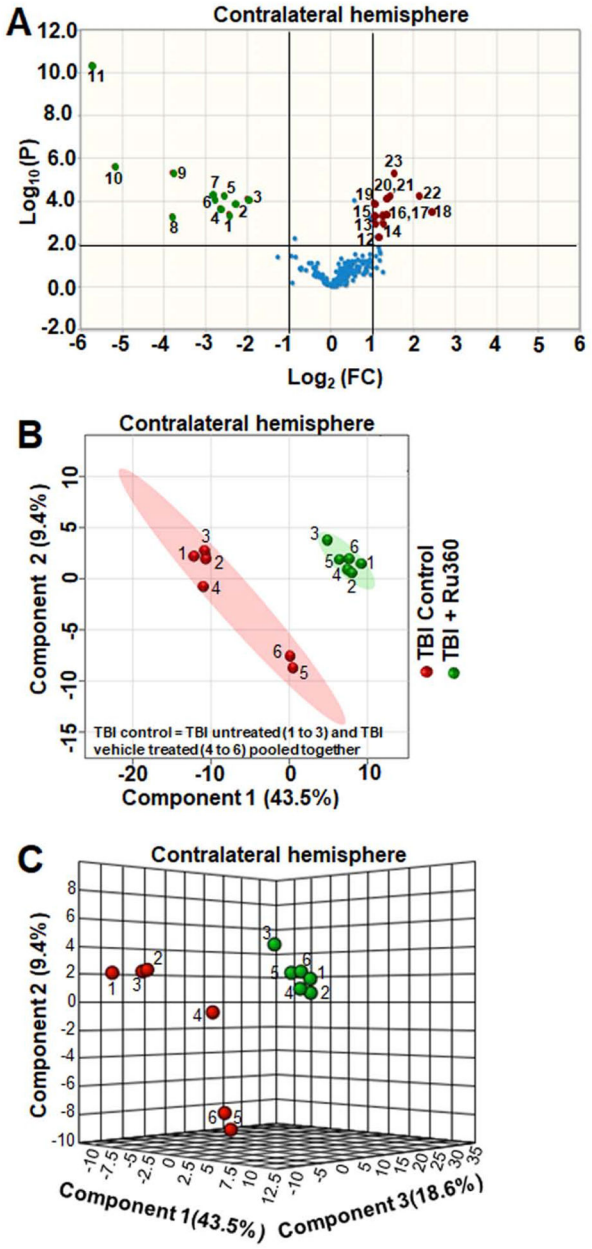

No	Metabolite
1	NADP
2	N-acetylputrescine
3	Hexanoylcarnitine
4	Citric acid
5	AMP
6	Betaine
7	Propionylcarnitine
8	Acetylcysteine
9	NAD
10	Phosphoenolpyruvic acid
11	Dimethylglycine
12	Uric acid
13	Phenylacetylglycine
14	Caprylic acid
15	Phenyllactic acid
16	Oxaloacetic acid (OAA)
17	Quinolinic acid
18	Glucose-6-phosphate
19	Nicotinic acid
20	Methylacetoacetic acid
21	Choline
22	L-histidinol
23	Pyruvic acid

Figure 5. Ru360 treatment on the contralateral hemisphere TBI metabolome

A) Volcano plot showing fold changes (FC) on the x-axis and FDR adjusted p-values on the y-axis. Black vertical and horizontal lines reflect the threshold criteria (FC=1.0 and $p<0.05$). Green and red dots represent metabolites significantly increased or decreased after Ru360 treatment respectively. 12% of the metabolites significantly changed between TBI+Ru360 treated (n=6) versus control TBI animals (n=6). Table on the right indicates changed metabolites as numbered in the volcano plot on the left panel. **B**) PLS-DA 2D scores plot and **C**) PLS-DA 3D scores plot respectively, indicating a complete class separation between Ru360 treated TBI animals (green dots) versus control TBI animals (red dots) with a tight clustering of the TBI metabolome across the Ru360 treated animals.

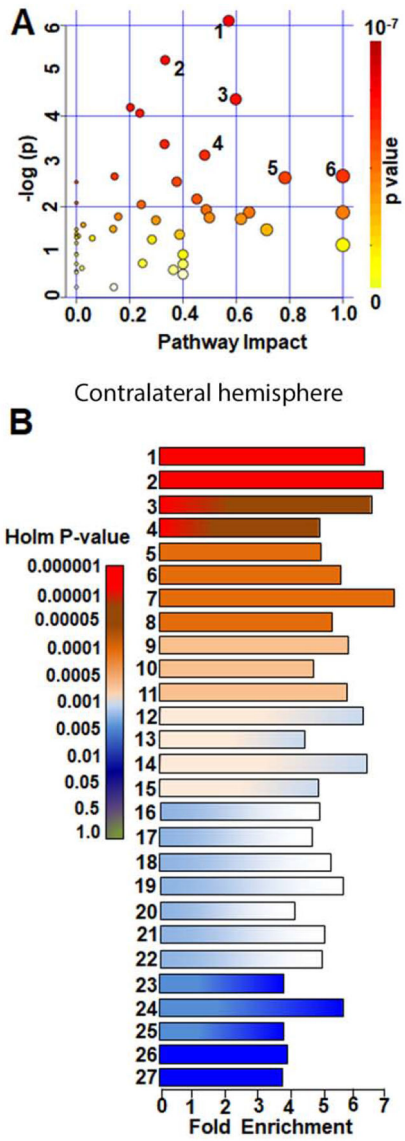

No	Metabolic pathway/Metabolism	P value	Holm P	FDR	Impact
1	Nicotinate and nicotinamide	0.0000002	0.00001	0.00002	0.57
2	Citric acid cycle	0.000002	0.00009	0.00004	0.33
3	Glycine, serine and threonine	0.00001	0.0008	0.0002	0.59
4	Glyoxylate and dicarboxylate	0.0003	0.01	0.002	0.48
5	Alanine, aspartate and glutamate	0.001	0.05	0.006	0.78
6	Valine, leucine and isoleucine biosynthesis	0.001	0.05	0.006	0.99

No	Metabolite set	P value	Holm P	FDR
1	Betaine metabolism	0.00000009	0.000003	0.000001
2	Lipid metabolism	0.0000001	0.000003	0.000001
3	Pyruvate metabolism	0.0000005	0.00001	0.000006
4	Methionine metabolism	0.0000007	0.00002	0.000006
5	Tryptophan metabolism	0.000005	0.0001	0.00003
6	Citric acid cycle	0.000009	0.0002	0.00005
7	Transfer of acetyl groups into mitochondria	0.00001	0.0002	0.00005
8	Phenylalanine and tyrosine metabolism	0.00001	0.0003	0.00005
9	Gluconeogenesis	0.00002	0.0007	0.0001
10	Histidine metabolism	0.00003	0.0008	0.0001
11	Nicotinate and nicotinamide metabolism	0.00003	0.0008	0.0001
12	Glycolysis	0.00005	0.001	0.0001
13	Purine metabolism	0.00007	0.001	0.0002
14	Glucose alanine cycle	0.0001	0.003	0.0003
15	Pentose phosphate pathway	0.0001	0.003	0.0004
16	Glycine and serine metabolism	0.0002	0.004	0.0004
17	Oxidative and mitochondrial metabolism	0.0002	0.005	0.0005
18	Urea cycle	0.0003	0.005	0.0005
19	Cardiolipin biosynthesis	0.0003	0.005	0.0005
20	Tyrosine metabolism	0.0003	0.005	0.0006
21	Phospholipid biosynthesis	0.0003	0.005	0.0006
22	Glutamate metabolism	0.0003	0.005	0.0006
23	Oxidation of branched chain fatty acids	0.0007	0.009	0.001
24	Malate-aspartate shuttle	0.001	0.01	0.001
25	Arginine and proline metabolism	0.002	0.01	0.002
26	Glutathione metabolism	0.008	0.04	0.009
27	Vitamin B6 metabolism	0.01	0.04	0.01

Figure 6. Pathway analysis of control versus Ru360 treatment on the contralateral hemisphere

A) Left-panel: Pathway analysis using MetPA with node colors indicating uncorrected p-values and node size the pathway impact values. Right-panel: Table showing significantly changed metabolic pathways with a threshold of $p<0.05$ for the corrected Holm p-value. **B**) Left-panel: MSEA results with y-axis indicating the significantly different metabolite sets based on a threshold of $p<0.05$ for the Holm p-value and color scaled to the corrected Holm p-value and x-axis indicating the respective fold enrichment. Right-panel: Table showing affected pathways relevant to the significantly enriched metabolite sets determined by MSEA.

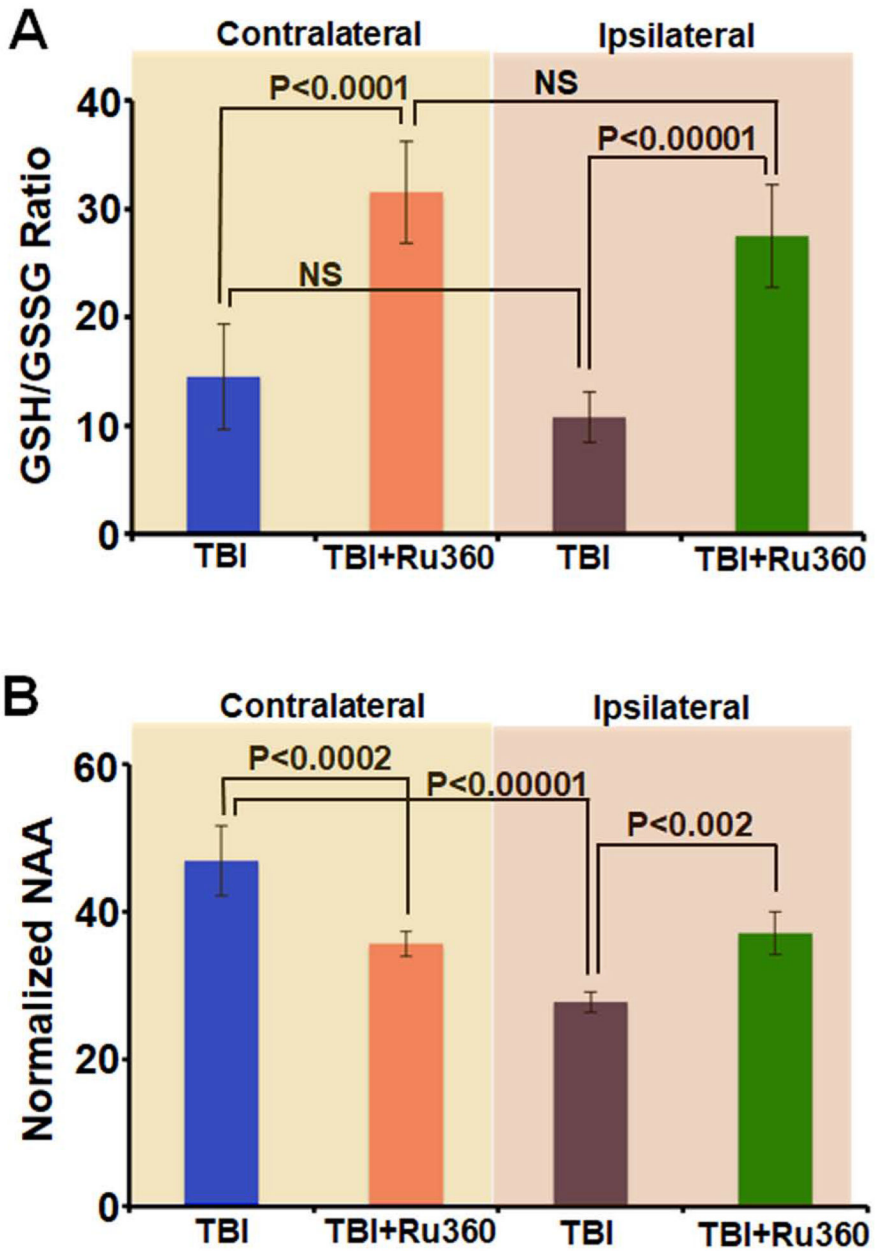

Figure 7. N-acetyl aspartate (NAA) levels and glutathione redox ratio

A) Reduced to oxidized glutathione ratio (GSH/GSSA) across the contralateral and ipsilateral hemispheres in the control TBI animals (n=6) and Ru360 treated TBI animals (n=6). **B)** NAA levels across the contralateral and ipsilateral hemispheres in the control TBI animals (n=6) and Ru360 treated TBI animals (n=6). Significance determined by one-way ANOVA with repeated measures. Data represent mean±SD.

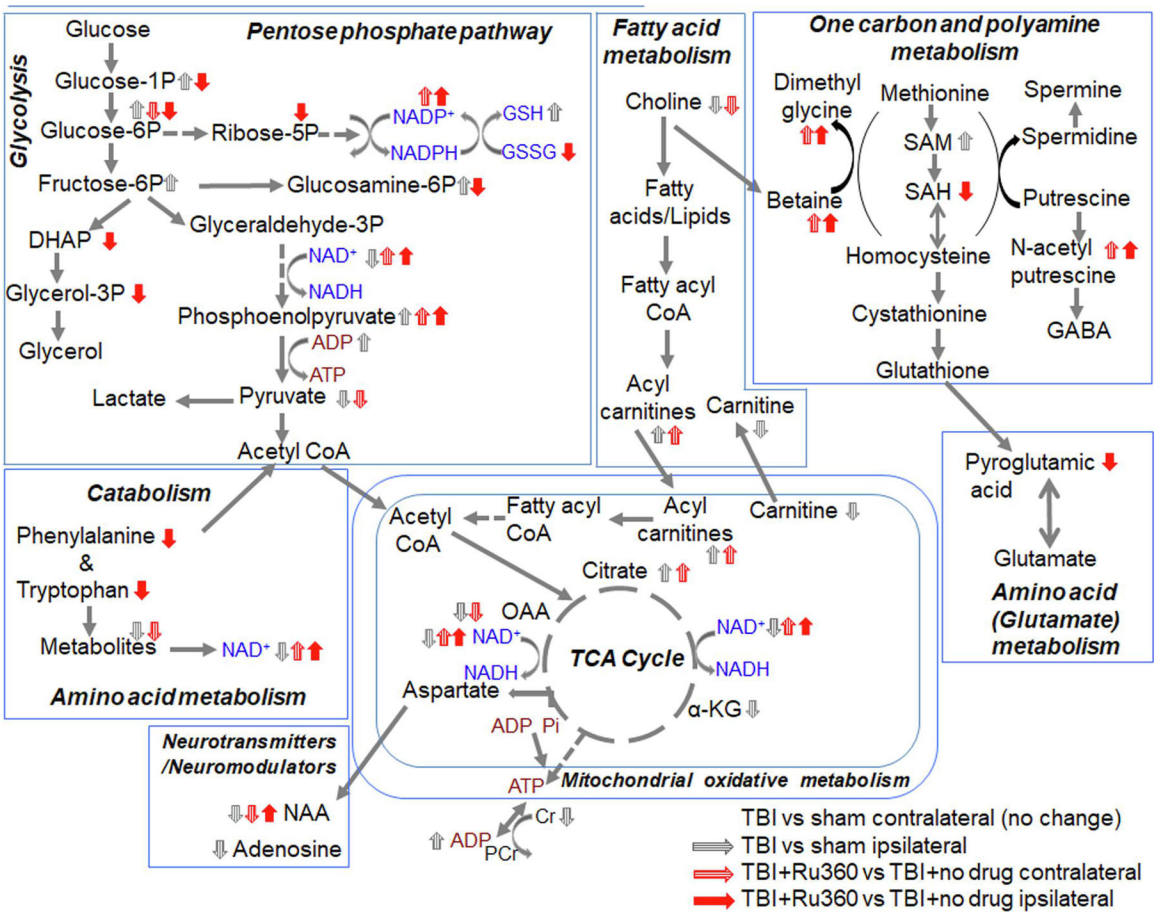

Figure 8. Schematic of biochemical pathways and metabolite changes.

Metabolites affected by TBI when compared to sham from our prior study on this TBI model (Chitturi, Li et al. 2018) and Ru360 treatment vs no drug effects on the TBI brain across the ipsilateral and contralateral hemispheres. Arrow directions indicate significant increase (↑) or decrease (↓) in metabolites ($P<0.05$; FDR corrected). No significant change was observed in any metabolite across the contralateral hemisphere after TBI when compared to contralateral sham (Chitturi, Li et al. 2018).